

## Model parameters of the nonlinear stiffness of the vibrator-ground contact determined by inversion of vibrator accelerometer data

Andrey V. Lebedev<sup>1</sup>, Igor A. Beresnev<sup>2</sup>, and Pieter L. Vermeer<sup>3</sup>

### ABSTRACT

Analysis of vibroseis data shows that harmonic distortion in the ground-force signal may exceed the primary distortions in the hydraulic system. This can be explained by the baseplate-ground contact nonlinearity created by the deformations of the contact roughness. We separated the nonlinear distortion generated in the hydraulics from that generated at the contact. We then formulated an inverse problem for resolving the parameters of the nonlinear contact rigidity, based on the equivalent model of the nonlinear source and the comparison of predicted and observed harmonic levels. The inverse problem was solved for models of bilinear contact and the contact with the rigidity smoothly varying between two asymptotic values, using data obtained on sandy soil. Rigidities changing between approximately  $10^9$  N/m in compression and  $6 \times 10^8$  N/m in tension were resolved from the inversion for both models, although the smooth nonlinear-rigidity model is a better approximation. The analysis shows the adequacy of the equivalent mechanical source model used for the description of nonlinear distortions in real soil-baseplate coupled systems.

### INTRODUCTION

Understanding and control of an outgoing signal are important for optimizing the vibrator performance and obtaining high-quality seismic data (Allen, 1996; Allen et al., 1998; Ghose et al., 1998; van der Veen et al., 1999; Lebedev and Malekhanov, 2003). Contact nonlinearity in the soil-baseplate system can lead to distortions in radiated signals and lags in crosscorrelations (Lebedev and Beresnev, 2004), which negatively affect data quality. Although the importance of properly accounting for nonlinear contact phenom-

ena to improve seismic data quality is recognized (e.g., Jeffryes, 1996; Ghose, 2003), determinations of the parameters of nonlinear stiffness of the ground, which could be used in source modeling, have been lacking. Our paper fills this gap by addressing the possibility of describing baseplate-measured acceleration data by two nonlinear contact-rigidity models: the bimodular contact (Lebedev and Beresnev, 2004) and the hyperbolic contact. The rigidity parameters are obtained from these two models by the inversion of measured data.

Nonlinear distortions of vibroseis signals arise from two mechanisms: hydraulic actuation and ground nonlinearity. For hydraulic vibrators, the actuator force itself typically carries a significant amount of harmonic distortion (e.g., Merritt, 1967). The algorithm designed to resolve the harmonics created by the contact nonlinearity must therefore be able to separate these two independent sources of nonlinearity. In inverting the real data, the primary distortions from the hydraulic system must first be recognized and then used as input to the baseplate. Additional distortion created by the nonlinear contact can then be resolved, from which the rigidity parameters can be calculated.

This paper is organized as follows. First, we introduce the two models of nonlinear contact rigidity and explain a possible way of separating nonlinear distortions resulting from the hydraulic system and the contact area alone. Then, field data are described and a realistic form of the actuator force is determined. Next, we discuss the algorithm of the inverse-problem solution, present the results of synthetic tests, and invert real vibroseis data. Finally, we compare the results obtained for the bimodular and hyperbolic models.

### MODEL FORMULATION — BIMODULAR AND SMOOTH PROFILES OF CONTACT RIGIDITY

A microscopically rough surface at the contact between the baseplate and the soil may result in an effective rigidity that varies with the load, leading to nonlinearity in the restoring force. The nature of the contact nonlinearity could be illustrated as follows. Soil

Manuscript received by the Editor April 15, 2005; revised manuscript received October 14, 2005; published online May 24, 2006.

<sup>1</sup>Iowa State University, Department of Geological and Atmospheric Sciences, 253 Science I, Ames, Iowa 50011-3212, and Russian Academy of Sciences, Institute of Applied Physics, 46 Ulyanov Street, Nizhny Novgorod, 603950 Russia. E-mail: swan@hydro.appl.sci-nnov.ru.

<sup>2</sup>Iowa State University, Department of Geological and Atmospheric Sciences, 253 Science I, Ames, Iowa 50011-3212. E-mail: beresnev@iastate.edu.

<sup>3</sup>WesternGeco, Oslo Technology Center, Schlumberger House, Solbråveien 23, 1370 Asker, Norway. E-mail: vermeer@oslo.westerngeco.slb.com.

© 2006 Society of Exploration Geophysicists. All rights reserved.

is a structurally inhomogeneous material that is in contact with the baseplate along a rough, uneven surface. The vibrations of the plate lead to the consecutive openings and closures of the contact points, so that the total contact surface is changing constantly (Solodov, 1998). This leads to variations in an effective elastic modulus of the contact. Furthermore, the contact region is typically much softer than the other parts of the interacting bodies (the baseplate and the consolidated material below); as a result, the deformations in this intermediate region are large enough to change the spectrum of radiation considerably. A model of such a contact and its effect on radiation were discussed by Lebedev and Beresnev (2004).

In the equivalent scheme of the vibroseis source (Lerwill, 1981; Sallas and Weber, 1982; Sallas, 1984; Safar, 1984), this nonlinearity can be accounted for by introducing a contact spring with the rigidity  $K_c = -dF_c/dx$  (Lebedev and Beresnev, 2004), where  $x \equiv z_2 - z_3$ ,  $F_c$  is the restoring force from the contact deformation, and  $z_1$ ,  $z_2$ , and  $z_3$  are the displacements of the reaction mass, baseplate, and the ground beneath the plate, respectively (Figure 1). The system of equations governing the source then becomes (Lebedev and Beresnev, 2004)

$$M_r \ddot{z}_1 + D_a(\dot{z}_1 - \dot{z}_2) + K_a(z_1 - z_2) = -F_a(t), \quad (1a)$$

$$M_b \ddot{z}_2 - D_a(\dot{z}_1 - \dot{z}_2) - K_a(z_1 - z_2) - F_c = +F_a(t), \quad (1b)$$

$$M_g \ddot{z}_3 + D_g \dot{z}_3 + K_g z_3 + F_c = 0, \quad (1c)$$

where  $M_r$  is the reaction mass;  $M_b$  is the baseplate mass;  $M_g$  is the captured mass describing the inertia of soil particles near the base-

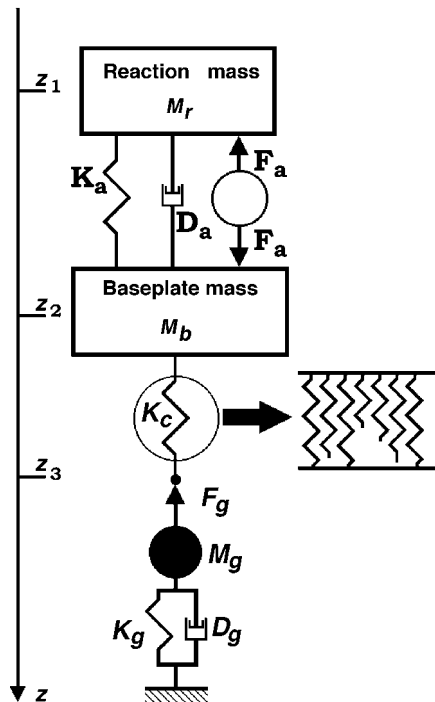


Figure 1. An equivalent scheme to model the nonlinear oscillations of the coupled ground-vibrator system. The scheme coincides with that used by Sallas (1984), except for the element  $K_c$ , which denotes an additional spring corresponding to the nonlinear contact rigidity. The horizontal arrow shows the model of the contact. The small springs have various heights; some of them are activated by vibrations. See text for other notations.

plate;  $D_a$  is the dashpot constant for the airbag suspension of the reaction mass, accounting for the corresponding losses;  $D_g$  is the dashpot constant, accounting for the losses attributable to seismic radiation;  $K_a$  is the actuator spring constant;  $K_g$  is the captured-spring constant describing the elastic response of the soil beneath the baseplate; and  $F_a(t)$  is the actuator force produced by the hydraulic system. Note that the use of the lumped parameters  $M_g, D_g$ , and  $K_g$  to describe the ground reaction is limited to low frequencies at which the baseplate size is small compared to radiated wavelengths (Gladwell, 1968). Otherwise, a more general concept of radiation impedance should be used (Miller and Pursey, 1954; Lebedev and Beresnev, 2005). If the rigidity  $K_c(x)$  is ascribed a specific functional form (the rigidity profile), a particular contact-nonlinearity model is introduced. All of the parameters entering equations 1 except the contact rigidity are considered to be known (e.g., Table 1 for sandy soil). Thus, the inverse problem discussed below is used to determine the contact-rigidity parameters only.

Rudenko and Vu (1994) propose modeling nonlinear contact rigidity by a set of springs of variable lengths, some being out of contact with the ground at a given deformation  $x$  (inset in Figure 1). This phenomenological model can describe a wide range of nonlinear contact behavior, including the Hertz point contact and a full contact (Johnson, 1985). By introducing a distribution of spring lengths (ground-roughness heights), varying degrees of nonlinearity can be accounted for. If the contact is complete (infinitely stiff), no deformation of the springs occurs and  $z_2 = z_3$ . This reduces equations 1 to the linear vibroseis model (Lerwill, 1981; Sallas and Weber, 1982; Safar, 1984; Sallas, 1984).

We will use two rigidity profiles. The first is the model of bimodular contact as considered by Lebedev and Beresnev (2004). It is depicted by the curves marked 1 in Figure 2 and is described as

Table 1. Vibroseis parameters used in the calculations. The captured parameters of the ground are as given by Safar (1984) for sandy soil, the actuator constants are as provided by Lerwill (1981).

$M_r$ (kg)	$M_b$ (kg)	$M_g$ (kg)	$K_a$ (N/m)	$K_g$ (N/m)	$D_a$ (kg/s)	$D_g$ (kg/s)
6963	1924	1236	$6.25 \times 10^5$	$7.69 \times 10^8$	$10^3$	$2.15 \times 10^6$

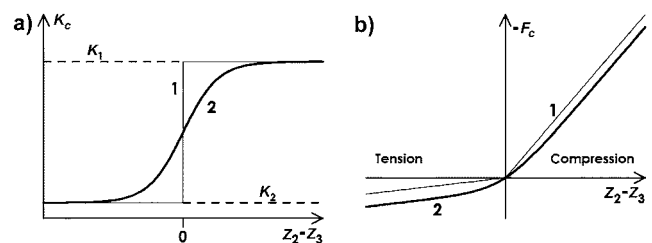


Figure 2. A schematic of (a) the rigidity profiles and (b) restoring force at the contact region. The curves 1 and 2 describe the bimodular rigidity and smooth rigidity given by equations 2 and 5, respectively.

$$K_c(x) = \begin{cases} K_1, & x > 0, \\ K_2, & x \leq 0, \end{cases} \quad (2)$$

where  $K_1 \geq K_2$  and  $x > 0$  corresponds to the compression under the plate. If the two rigidities are equal, the contact is linear and no distortions occur. Equation 2 corresponds to the microsprings of two lengths in Figure 1, meaning that, in the compression phase, all microsprings are active, while in the tension only the longer ones are deformed. The restoring force is determined as an integral of  $K_c$  over deformation  $x$ ,

$$F_c(x) = - \int_0^x K_c(y) dy, \quad (3)$$

or

$$F_c(x) = \begin{cases} -K_1 x, & x > 0, \\ -K_2 x, & x \leq 0. \end{cases} \quad (4)$$

The second rigidity function is a smooth (hyperbolic-tangent) profile saturating at both large compression and tension. This corresponds to the case when there are many microsprings of variable length and all of them are activated upon reaching a certain compression value, while only one remains active beyond a certain tension. The corresponding functional form is

$$K_c(x) = K_2 + \frac{K_1 - K_2}{2} \left[ \tanh\left(\frac{x}{d}\right) + 1 \right], \quad (5)$$

where  $d$  is the characteristic deformation scale (curve 2 in Figure 2a). The parameter  $d$  is a quantitative measure of nonlinearity in  $K_c$  controlling the width of the transition zone in which the rigidity changes between the asymptotic values of  $K_1$  and  $K_2$ ; the cases of  $d \rightarrow \infty$  and  $d \rightarrow 0$  correspond to the linear (infinite width, constant rigidity) and bimodular (zero width, instant switch between rigidities) contacts, respectively. Physically, it can be viewed as a characteristic length scale of microspring activation. Equation 5 thus encompasses equation 2 as a limiting case. The restoring force in equation 5 is

$$F_c = -K_2 x - \frac{K_1 - K_2}{2} \left[ d \ln \cosh\left(\frac{x}{d}\right) + x \right] \quad (6)$$

(see Figure 2b).

We remind the reader that in the model described by the set of equations 1, the force applied to the ground is  $-F_g = M_g \ddot{z}_3 + D_g \dot{z}_3 + K_g z_3$ , where  $F_g$  is the ground-reaction force. The ground-reaction force can be calculated in a standard way (e.g., Sallas and Weber, 1982):

$$F_g \equiv F_c = M_r \ddot{z}_1 + M_b \ddot{z}_2. \quad (7)$$

We have already pointed out that, apart from the nonlinear distortions in the contact area, there exist initial distortions in the hydraulic system. In the set of equations 1, the hydraulic source of distortions can be accounted for by using a nonsinusoidal time history for the actuator force  $F_a$ . The standard vibroseis field measurements involve the recordings from two accelerometers, one mount-

ed on the reaction mass and one on the baseplate. It is therefore necessary to determine the input actuator force using only the data from these two reference sensors.

We see from equation 1a that

$$-M_r \ddot{z}_1 - D_a(\dot{z}_1 - \dot{z}_2) - K_a(z_1 - z_2) = F_a(t). \quad (8)$$

If the parameters entering equation 8 are known, the actuator force can be determined using the reference-accelerometer recordings. However, since the first term in the left-hand side of this formula grows as the square of the frequency, it will dominate the remaining two terms in the seismic frequency band (practically, above the reaction-mass resonance  $\omega_1 = \sqrt{K_a/M_r}$ ). The actuator force then is

$$F_a(t) \approx -M_r \ddot{z}_1, \quad (9)$$

which can be directly calculated from the readings of the reaction-mass accelerometer. Because the reaction-mass resonance lies at 1–3 Hz, equation 9 is satisfactory for the operating band of the vibroseis sources (10–100 Hz). For illustration, numeric simulation of the set of equations 1 for the lumped parameters specified in Table 1 and the contact rigidities found by the inversion show that the amplitude of the actuator force  $F_a$  approximated by equation 9 coincides with that of the exact sinusoidal input actuator force within approximately 1%, at the frequency of inversion of 48 Hz.

## DATA DESCRIPTION

The results of vibroseis measurements that we use were obtained on sandy soil on a vibrator with peak force of  $3.6 \times 10^5$  N (80 klbf). The experimental records comprise the reference-accelerometer readings on the reaction mass and the baseplate. The parameters of the vibroseis system used to solve equations 1 are given in Table 1. These parameters are needed to define the system for the inversion completely; the parameters inverted for are only those of the nonlinear rigidity profiles,  $K_1$  and  $K_2$  for equation 2 and  $K_1$ ,  $K_2$ , and  $d$  for equation 5. The vibrator ran at 60% of peak force, which provided good linearity in the hydraulic system. The vibrator swept from 10–90 Hz for a total duration of 19 s.

The ground-reaction force given by equation 7, which can be determined from the measurements, consists of two terms. At low frequencies, the first term  $M_r \ddot{z}_1$ , describing the actuator force in equation 10, prevails (Lerwill, 1981; Safar, 1984). For example, on sandy soil the second term is below approximately 10% of the first term in equation 7 up to frequencies of about 30 Hz (Lebedev and Beresnev, 2005). The nonlinear distortions in the ground force resulting from the contact phenomena are therefore expected to be masked by the hydraulic distortions. To reveal the distortions caused by the contact, higher frequencies should be analyzed. Choosing the starting time and the appropriate length of the time window makes it possible to analyze nearly tonal vibroseis radiation. We chose the window in the sweep that corresponds to the main tone of approximately 48 Hz. The frequency limit of the recording system is 250 Hz; in this case, up to five harmonics of the main tone can be incorporated into the analysis.

Figure 3 shows the measured harmonic content in the actuator force and the ground-reaction force determined according to equations 9 and 7, respectively. To select a window of the sweep corresponding to the main tone of approximately 48 Hz, a 128-sample segment of the sweep record was used (the full length of the record

was 9500 samples with a sampling interval of 0.002 s). To increase the frequency resolution, the segment was padded with zeros to the length of 8192 samples. This explains the side lobes of the main tone and the harmonics seen in Figure 3.

Figure 3 shows that the ground force is clearly more distorted than the actuator force. It is important to note, though, that nonlinear system 1 may exhibit internal resonances at the frequencies that are not known a priori; therefore, one cannot rule out the possibility that the larger ground-force distortion observed comes from the amplification by the system's internal transfer function. Although the relative harmonic distortion between the ground force and the actuator force seen in Figure 3 provides qualitative guidance, rigorous analysis of equations 1 is necessary to separate the harmonics resulting from the contact nonlinearity and use them in the inversion for the nonlinear contact rigidity parameters.

From equation 9 and the data spectrum, we obtain the harmonics of the distorted actuator signal:

$$F_a(t) = F_0 \sum_{n=1}^3 a_n \sin(n\omega t + \varphi_n),$$

$$a_1 = 1, a_2 = 0.0591, a_3 = 0.0202,$$

$$\varphi_1 = 0, \varphi_2 = -76.68^\circ, \varphi_3 = 78.61^\circ, \quad (10)$$

where the amplitudes  $a_n$  are normalized by the peak force  $F_0 = 2.2 \times 10^5$  N [60% of the maximum force of the  $3.6 \times 10^5$  N (80 klbf) vibrator]. The harmonics higher than  $n = 3$  in the actuator force were not observed in the original spectra (Figure 3). Note that, in the model of bimodular nonlinearity given by equation 2, the exact value of  $F_0$  does not affect the values of  $a_n$  because the harmonic distortion at the baseplate-ground contact in this model does not depend on the force amplitude (Lebedev and Beresnev, 2004). This is not true for equation 5, in which  $F_0$  will affect the harmonic amplitudes.

## INVERSE PROBLEM SOLUTION

The distorted actuator force determined by equation 10 is substituted into equations 1, and the equations are solved numerically us-

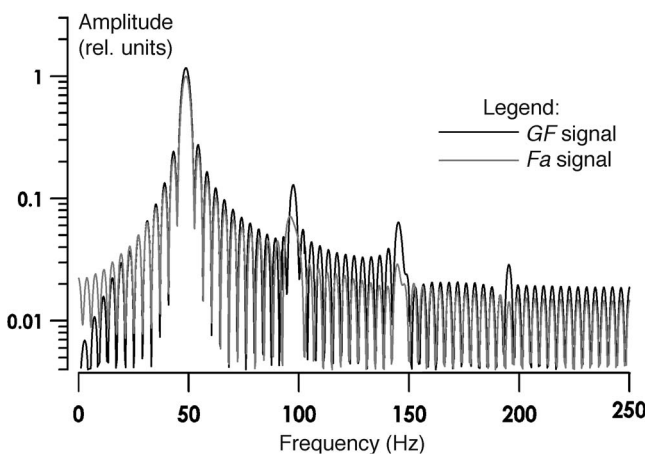


Figure 3. Comparison of harmonic content in the ground-force  $F_g$  and actuator-force  $F_a$  signals. The main tone is approximately 48 Hz. The ordinate values were chosen to equal unity at the actuator main tone.

ing the Runge-Kutta scheme, as explained by Lebedev and Beresnev (2004). Then we use the parameters of the vibroseis system as in Table 1 for the respective model of the restoring force in equations 4 or 6 to find the model predictions of  $z_j$  for  $j = 1, 2, 3$  and their time derivatives. The experimental data are the reference-accelerometer readings, and the ground force is defined by equation 7.

The nonlinear rigidity of the contact leads to the generation of higher harmonics in the ground force. We can therefore compare the experimentally measured levels with the predicted relative harmonic levels in the ground force calculated using equation 7. Then, using the realistic actuator force determined by equation 10, we can adjust model parameters until the best fit is achieved. Fitting is conducted in the sense defined by the search algorithm, as a global minimum of the objective function, defined as the sum of the squared differences between the observed and the model-predicted relative harmonic levels (Appendix A). The relative harmonic levels are calculated by normalizing their spectral amplitudes by the total harmonic spectral power (the sum of their squared amplitudes). The details of the inversion algorithm are provided in Appendix A.

## SYNTHETIC TEST

We start with a synthetic numeric example to investigate the uniqueness of the solution of the inverse problem. The uniqueness means that the objective function A-1 (see Appendix A) has only one global minimum corresponding to a unique value of the parameter vector  $\mathbf{p}$ . The bimodular contact model (equation 2) is used with the parameter vector  $\mathbf{p} = \{K_1, K_2\}$ .

Using equations 1 and 4, we calculate the synthetic harmonic distortion in the ground force for a given pair of contact rigidities,  $K_1^{\text{true}} = 10^{10}$  N/m and  $K_2^{\text{true}} = 10^9$  N/m, for the realistically recorded actuator force determined by equation 10. The normalized synthetic harmonic amplitudes are stored as experimental data  $l_n$  in the objective function A-1. The number of harmonics used is four, corresponding to their number, including the fundamental, seen in the measured ground force (Figure 3). We next perform a grid-search inversion of the synthetic data to find  $K_1$  and  $K_2$  that minimize the objective function, over the square grid in  $K_1$  and  $K_2$ , each changing from  $10^8$  to  $2 \times 10^{10}$  N/m, with a uniform 10% increment (a factor of 1.1) in the rigidity logarithm (56 points on each side of the grid). We finally check if the result of the inversion (the values of  $K_1$  and  $K_2$  that minimize the objective function) converges to the known  $K_1^{\text{true}}$  and  $K_2^{\text{true}}$ . The computer time for a topography plot of the objective function described is about 3 hours on a Pentium IV computer with a 2-GHz processor. The direct grid search is thus computationally demanding.

Figure 4 shows the topography of the objective function  $\varepsilon(K_1, K_2)$  over the search grid. By definition, the rigidity in compression is always greater than or equal to that in tension; the region  $K_2 > K_1$  is therefore arbitrarily set to a plateau. The point on the grid corresponding to  $\mathbf{p}^{\text{true}} = \{K_1^{\text{true}}, K_2^{\text{true}}\}$  (the known true solution) is shown as the green dot.

The region of the minimum in the relief appears as a narrow valley; the global minimum of  $\varepsilon(K_1, K_2)$  within the search grid should therefore be expected within this valley. To investigate the latter's fine structure, we calculated the objective function with a smaller 1% increment in  $K_j$  over the respective area. The enlarged view of this smaller area is shown in Figure 5a, where we find a more com-

plex topography with one additional local minimum away from the true solution. The presence of such a minimum implies that the gradient-minimization method described in Appendix A may provide false values of  $K_j$  if an inappropriate initial approximation is chosen. This possibility is illustrated in Figure 5a by the red and cyan arrows indicating the descent areas for the global (red) and local (cyan) minima. The numbers show the different initial approximations made:  $K_1^{[1]} = 8 \times 10^9, 3 \times 10^9, 3 \times 10^9, 4 \times 10^9, 2.5 \times 10^9$  N/m and  $K_2^{[1]} = 1.15 \times 10^9, 8 \times 10^8, 7 \times 10^8, 1.1 \times 10^9, 7 \times 10^8$  N/m for cases 1–5, respectively. The  $K_1^{[1]}-K_2^{[1]}$  pairs were chosen not to be close to the global minimum. Points 1 and 4 lie far from the saddle separating the global and the local minima, for which we can expect a rather quick convergence. Points 2 and 3 are close to the saddle; a slightly slower convergence results. Point 5 is located in the attraction area of the local minimum, illustrating the possibility of obtaining a false solution. This suggests the necessity of a preliminary investigation of the global minimum during the grid search.

Figure 5b reproduces the relief near the global minimum for the case when the hydraulic system is linear and provides no distortion in the actuator force. The local minimum disappears, while the structure of the global minimum remains virtually unchanged. The local minimum in Figure 5a is consequently the result of the interference of the primary harmonics with those occurring in the soil-baseplate system. This effect has a clear explanation. The interference occurs in such a way that the observed distortion in the ground force can be reproduced by different combinations of the contact rigidities, in addition to the true solution.

The shape of the valley in Figures 4 and 5 outlines the region of uncertainty in determining the rigidities  $K_j$ . The shape is elongated along  $K_1$  and narrow along  $K_2$ , implying that we can expect a greater ambiguity in determining the compression rigidity  $K_1$  than the tension rigidity  $K_2$ . Mathematically, this shape is controlled by the values of the derivative  $\partial L_n(\mathbf{p}^{[m]})/\partial p_k$  in equation A-3, such that the derivative is small along  $K_1$  and large along  $K_2$ . Thus, a quantitative criterion is introduced for the standard deviation  $\delta p_k$ , expressed in equation A-5, of each estimated parameter  $p_k$ . The uncertainty  $\delta p_k$  of the inversion is the same if an appropriate initial

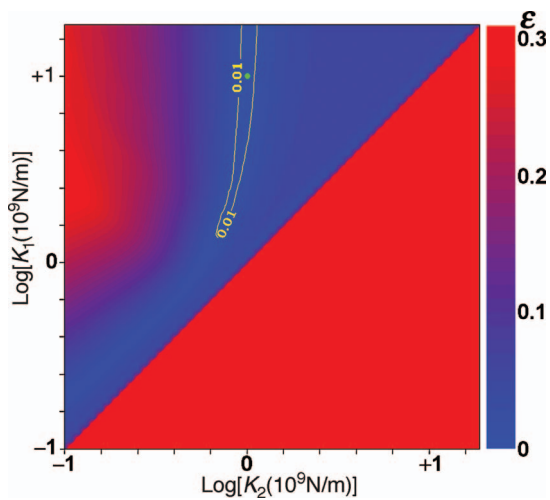


Figure 4. Topography of the objective function A-1 (sum of the squared differences between observed and model-predicted relative harmonic levels) over the grid of rigidities. Logarithms are base 10.

approximation is used (cases 1–4 in Figure 5):  $K_1 = (1 \pm 1.6 \times 10^{-5}) \times 10^{10}$  N/m and  $K_2 = (1 \pm 7 \times 10^{-6}) \times 10^9$  N/m. Evidently, the errors are small enough to be neglected; in the absence of noise, they are chiefly caused by the numeric errors introduced when calculating the derivatives. In the case of a descent into the local minimum (case 5 in Figure 5), the uncertainty is much greater,  $K_1 = (1.7 \pm 0.1) \times 10^9$  N/m and  $K_2 = (7.5 \pm 0.2) \times 10^8$  N/m, which can be considered an indication of solution failure.

The results presented in Figures 4 and 5 were derived from the synthetic data without noise. Note that even if the theoretical model is a good approximation of the measurements, the presence of noise may blur the appearance of the global minimum. Our numeric experiments showed that the noise level should be comparable to the amplitudes of the second and third harmonics to significantly degrade the identification of the global minimum. When the recordings are made on the baseplate with high S/N as in Figure 3, such large noise levels typically do not occur.

We conclude that the combination of a thorough grid search and the local gradient search to minimize objective function A-1 provides, at least in the test case considered, the global minimum that converges to the true solution.

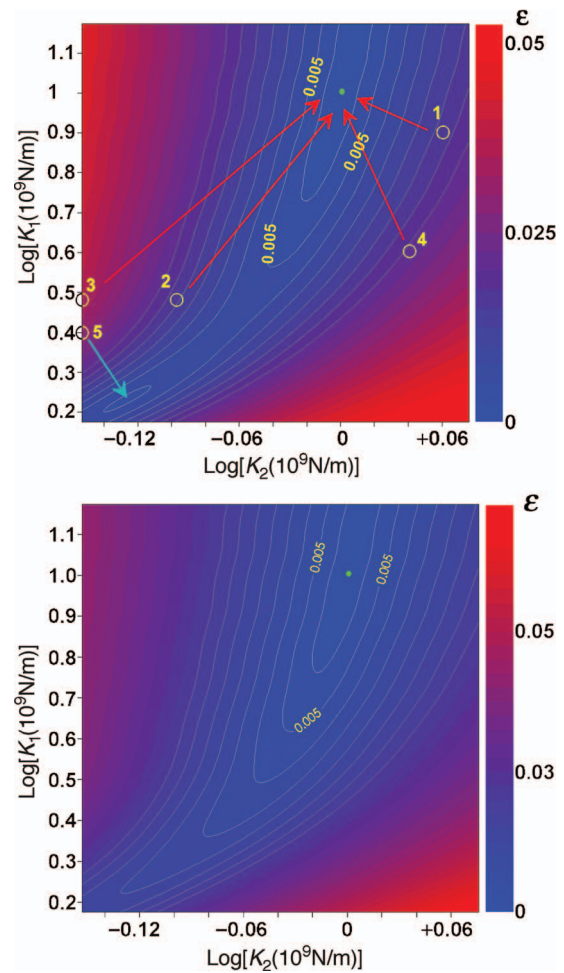


Figure 5. Fine structure of the objective function A-1 near the global minimum. See text for notations. (a) Nonlinear actuator force determined from equation 10. (b) Linear actuator force (tonal excitation).

### VIBROSEIS DATA INVERSION

Figure 6 shows the topography of the objective function obtained using equation 2 and real experimental data. The limiting values of the rigidities in the search grid correspond to the case of a well-prepared contact (Lebedev and Beresnev, 2004). We see that the function has a global minimum within this grid at approximately  $K_1 = 10^9$  N/m and  $K_2 = 7 \times 10^8$  N/m. Many local minima are also seen; their alignment along the diagonal line on the map indicates the contact system in the experiment was close to being linear; however, the model of bilinear contact (the global minimum) still provided a better fit to the data.

The refined search by the gradient method, started from  $K_1 = 10^9$  N/m and  $K_2 = 7 \times 10^8$  N/m, close to the minimum found by the grid search, gave solutions after four iterations of  $K_1 = (1.09 \pm 0.14) \times 10^9$  N/m and  $K_2 = (6.64 \pm 0.49) \times 10^8$  N/m. The accuracy of the parameter estimation is thus 7%–13%. To be sure that the global minimum was found in the grid, we carried out an additional gradient search for several other initial pairs,  $K_1 = 2.5 \times 10^9, 1.6 \times 10^9, 0.9 \times 10^9, 0.7 \times 10^9$  and  $K_2 = 1 \times 10^9, 0.5 \times 10^9, 0.7 \times 10^9, 0.4 \times 10^9$  N/m, respectively (shown as the blue dots with arrows in Figure 6). With a slight difference in the required number of iterations, the final values of the rigidities were found to be the same.

Figure 7 shows the measured relative harmonic levels and those calculated for the parameters found (black solid line). The error in the measured values was estimated from the noise in the spectra of experimental records. It can be seen from Figure 3 that the spectral level above approximately 200 Hz are at a constant level of about 0.02, the amplitude of the fundamental. This level, normalized by the total harmonic spectral power, is indicated by the empty circle in Figure 7. It quantifies the uncertainty in the determination of harmonic amplitudes and constitutes the length of the error bars for the measured values. We see that the model of bimodular rigidity provides a satisfactory, but not perfect, fit to the data.

As pointed out by Lebedev and Beresnev (2004), the bimodular-rigidity model is an approximation that does not account for a possible dependence of harmonic distortion on the amplitude of the actuator force. This dependence could be incorporated by utilizing smooth, nonlinear functions of rigidity versus strain. The hyper-

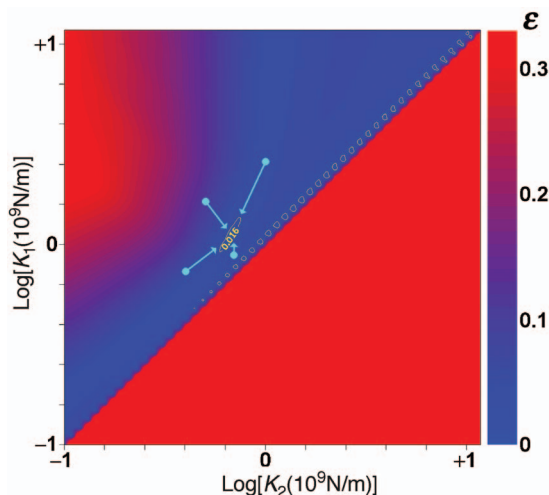


Figure 6. Topography of the objective function A-1 obtained with experimental data. See text for notations.

bolic-tangent profile (equation 5) is such a generalization. It would be instructive to see if this generalized rigidity could better fit the vibroseis data. Strictly speaking, a thorough evaluation of equation 5 would involve experimental data obtained at various amplitudes of the actuator force. One then could invert for a set of parameters  $\{K_1, K_2, d\}$  for each actuator-force value. If equation 5 were valid, all sets of parameters would be the same within the respective error bounds.

We do not possess experimental data for various levels of the applied force, having the data for the actuator force of  $F_0 \approx 2.2 \times 10^5$  N. We therefore can only find one set of parameters  $\{K_1, K_2, d\}$ ; however, we still could verify if they fit the experimental data better than the bimodular parameters. The inversion parameters that we determined for the hyperbolic model are  $K_1 = (1.45 \pm 0.04) \times 10^9$  N/m,  $K_2 = (5.52 \pm 0.05) \times 10^8$  N/m, and  $d = (2.76 \pm 0.03) \times 10^{-4}$  m. The calculated relative harmonic levels for the hyperbolic model are shown in Figure 7 by the gray line. We infer that the rigidity values for equations 5 and 2 are similar and that the value of  $d$  is small enough for the contact to be considered close to bimodular. The latter can be seen directly by calculating the extreme values of  $|z_2 - z_3|/d$ , which span both asymptotic rigidity levels in equation 5.

We do see, however, that the hyperbolic rigidity profile provides a better fit to the observed harmonic levels (Figure 7, black and gray lines) and estimates the rigidity parameters more precisely. Also, the objective-function minimum is two orders of magnitude higher for the bimodular ( $\varepsilon_0 = 8.7 \times 10^{-4}$ ) than for the hyperbolic ( $\varepsilon_0 = 6.7 \times 10^{-6}$ ) model. We conclude that the bimodular contact generally provides a good approximation of the contact rigidity and can adequately capture the harmonic distortion in vibroseis signals. However, this example also shows that smooth nonlinear-rigidity profiles, such as the hyperbolic law, may prove more advantageous in explaining the data, which could further be verified by considering measurements at various force levels. On the other hand, the better fit for the case of equation 5 could simply be because of the larger number of parameters in the inversion while keeping the same number of experimentally observed harmonics of four only (including the main tone). Therefore, expanded experiments are required to distinguish the true benefit of equation 5.

### SOUNDNESS OF OBTAINED VALUES

For sandy soil beneath the baseplate, the macroscopic rigidities most probably result from the microscopic rigidities of Hertz-point

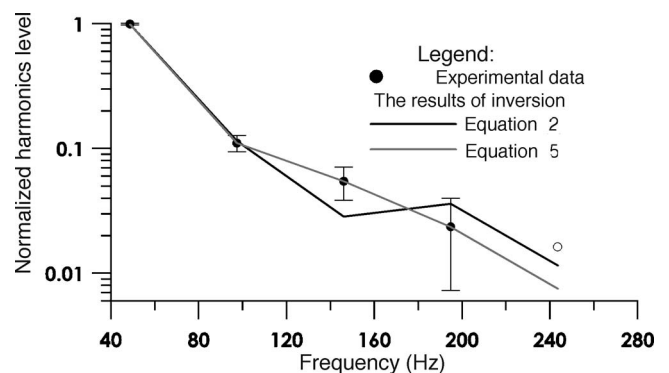


Figure 7. The relative level of harmonics. The experimental data are shown by circles and the results of inversion are solid lines. The empty circle corresponds to the spectral-noise level.

contacts of individual grains. In a packed-sphere rock model, the contact rigidity  $K_c$  between grains is related to the bulk modulus  $K$  of the medium as  $K = K_c/D$ , where  $D$  is the grain diameter (Sheriff and Geldart, 1995). Assuming a typical bulk modulus of  $10^9$  Pa ( $2 \times 10^9$  Pa is the bulk modulus of water) and a sand-grain diameter of  $10^{-3}$  m, we estimate the grain contact rigidity as  $10^6$  N/m. As it should be, it is much smaller than the estimated cumulative macroscopic rigidities under the plate, since they are controlled by the rigidities of multiple grains.

The relative displacement  $x$  of individual particles in response to a force  $F$  scales, independently of their shapes, as  $F^{2/3}$  (Landau et al., 1986). The definition of the contact rigidity then leads to the scaling of  $K_c \sim F^{1/3}$ . The force acting on the contact area consists of the static hold-down force and the dynamic ground force  $F_c$ . The hold-down force has the order of magnitude of the maximum design force of the vibrator  $3.6 \times 10^5$  N, and the ground force is on the order of the observed peak actuator force ( $2.2 \times 10^5$  N) [e.g., see values of  $|F_g/F_a|$  calculated theoretically by Lebedev and Beresnev (2004)]. The total force  $F$  that acts on the contact area in the experiment thus oscillates between approximately  $1.4 \times 10^5$  and  $5.8 \times 10^5$  N, corresponding to the compression and tension phases, respectively. The rigidities corresponding to these two force levels (deformation phases) should thus be approximately related as  $\sqrt[3]{5.8/1.4} \approx 1.6$ .

We have found  $K_1 = (1.09 \pm 0.14) \times 10^9$  N/m for the compression phase and  $K_2 = (6.64 \pm 0.49) \times 10^8$  N/m for the tension phase. Their ratio is thus estimated to be approximately between 1.3 and 2.0 with a mean value of 1.6, which conforms well to the value expected from the applied-force estimates.

Finally, the parameter  $d$  of the hyperbolic-tangent profile given by equation 5 is the characteristic length of the microspring activation. At deformations  $x = \pm 2d$ , function 5 reaches the asymptotic values of  $K_{1,2}$  within the accuracy of 2%. The length scale of  $4d = 4 \times 0.28 \approx 1.1$  mm thus describes the full swing in the contact-rigidity variation. This value should be and is compatible with the characteristic length scale of internal heterogeneity of the soil (the size of sand particles).

The values of the rigidities found are thus in reasonable agreement with the consequences of contact mechanics. More experiments, especially at variable applied-force levels, will of course allow us to establish the preference for a particular nonlinear contact-rigidity model and bracket the relevant parameters more precisely.

## SUMMARY

The analysis of experimental vibroseis data within the equivalent model of the nonlinear source revealed the clear presence of the harmonic distortion at the baseplate contact in addition to the primary distortions generated by the hydraulics. We solved an inverse problem for the determination of nonlinear contact-rigidity parameters based on the observed and predicted harmonic levels. The inversion produced contact rigidities for the bimodular model and the model in which they varied smoothly between two asymptotic values. We found compatible rigidity pairs for both models, consistent with the fact that the former is a limiting case of the latter, although the model of smooth amplitude-dependent rigidity may fit the harmonic levels better. To ascertain its preference for the description of the observed harmonic distortion, harmonics at variable peak actuator-force values should be analyzed. The mag-

nitudes of the rigidities are of the order expected from the relationships of the contact mechanics. The analysis showed the adequacy of the equivalent model (equations 1) for vibroseis data.

## ACKNOWLEDGMENTS

Funding and data for this work were provided by WesternGeco. We are indebted to three anonymous reviewers for valuable suggestions.

## APPENDIX A

### AN ALGORITHM FOR SOLVING THE INVERSE PROBLEM

Let us denote  $L_n(\mathbf{p})$  as the relative level of an  $n$ th harmonic predicted by the model for a particular vector of model parameters  $\mathbf{p}$  containing  $M$  values in question (e.g.,  $K_{1,2}$  and  $d$  in equation 5, that is,  $M = 3$ ), where  $L_n$  is a nonlinear operator. Also let  $l_n$  be the observed level of the harmonic. The solution of the inverse problem in an optimal (least-squares) sense in the presence of Gaussian noise is one that minimizes the residual (objective function)  $\varepsilon$  (Hudson, 1964):

$$\varepsilon = \sum_{n=1}^N w_n [L_n(\mathbf{p}) - l_n]^2, \quad (\text{A-1})$$

where  $N$  is the total number of the harmonics and  $w_n$  is the data weight. The simplest approach to the solution of the inverse problem would then be a search through the entire space of plausible parameters for the set that minimizes the residual. This grid-search procedure normally requires a high volume of calculations and, in our case, can be used with coarse increments in the parameter values to investigate the structure of the objective function and find its possible minima. To find the exact values of the best-fitting parameters, the search in the vicinity of the global minimum should be refined using a more efficient algorithm such as the gradient search.

The minimization of equation A-1 is equivalent to the solution of an overdetermined set of algebraic equations (Bard, 1974),

$$L_n(\mathbf{p}) = l_n, \quad n = 1, 2, \dots, N. \quad (\text{A-2})$$

The nonlinear minimization problem A-2 can be solved by standard iterative Newton-type gradient methods of (e.g., Korn and Korn, 1968). The method starts with an initial approximation for the components  $p_k^{[1]}$  of the parameter vector  $\mathbf{p}$ , which can be obtained by the grid search, where the subscript  $k$  is the parameter number ( $k = 1, \dots, M$ ) and the superscript is the iteration number. The residual A-1 for  $\mathbf{p}^{[1]}$  is calculated. The next  $[(m+1)$ th] approximation  $p_k^{[m+1]}$  is defined according to the Newton scheme by expanding the functions  $L_n(\mathbf{p})$  in equation A-2 into the Taylor series around  $p_k^{[m]}$  and retaining the linear term,

$$L_n(\mathbf{p}^{[m+1]}) = L_n(\mathbf{p}^{[m]}) + \sum_{k=1}^M \frac{\Delta p_k \partial L_n(\mathbf{p}^{[m]})}{\partial p_k}. \quad (\text{A-3})$$

The right-hand side of equation A-3 is substituted into equations A-2, yielding

$$L_n(\mathbf{p}^{[m]}) + \sum_{k=1}^M \frac{\Delta p_k \partial L_n(\mathbf{p}^{[m]})}{\partial p_k} = l_n, \quad (\text{A-4})$$

which is solved for  $\Delta p_k$ . The next approximation is  $p_k^{[m+1]} = p_k^{[m]} + \Delta p_k$ . The residual for  $p_k^{[m+1]}$  is calculated, and the process is continued until a minimum residual level  $\varepsilon_0$  is reached.

Since system A-4 is overdetermined (the number of unknown parameters  $p_k$  is generally smaller than the number of fitted harmonics  $N$ ), its solution is obtained in an optimal sense through the standard least-squares matrix inversion (e.g., Hatton et al., 1986).

When the global minimum of function A-1 is achieved, the standard deviations  $\delta p_k$  in the parameters  $p_k$  can be determined as (Bard, 1974)

$$\delta p_k = \sqrt{\frac{\varepsilon_0}{\sum_{n=1}^N w_n [\partial L_n(\mathbf{p}^{[m]}) / \partial p_k]^2}}, \quad (\text{A-5})$$

where the derivatives are obtained from the last iteration. For simplicity, the data weights  $w_n$  are set to unity. This means the reliability of harmonic amplitudes is the same for each harmonic (Hudson, 1964).

Note that the combination of the grid-search/gradient-search algorithms used in this study is well representative of known minimization approaches. For example, the so-called genetic or simulated-annealing algorithms are still variations of a grid search. These methods are used when the number of unknown parameters is relatively large and a more structured approach to random search is required. Such an approach is typically implemented by setting prescribed, often heuristic criteria for choosing the optimum search direction. They are just as vulnerable to falling to local minima (e.g., Liu et al., 1995). The approach taken is adequate to our problem, where the number of unknown parameters is two or three.

## REFERENCES

- Allen, K. P., 1996, High fidelity vibratory source seismic method: U.S. patent 5 550 786.
- Allen, K. P., M. L. Johnson, and J. S. May, 1998, High fidelity vibratory seismic (HFVS) method for acquiring seismic data: 68th Annual International Meeting, SEG, Expanded Abstracts, 140–143.
- Bard, Y., 1974, Nonlinear parameter estimations: Academic Press.
- Ghose, R., 2003, AVO analysis of shallow seismic horizons: Effect of accuracy and uniformity of the effective source wavelet: Annual International Meeting, SEG, Expanded Abstracts, 1239–1242.
- Ghose, R., V. Nijhof, J. Brouwer, Y. Matsubara, Y. Kaida, and T. Takahashi, 1998, Shallow to very shallow, high-resolution reflection seismic using a portable vibrator system, *Geophysics*, **63**, 1295–1309.
- Gladwell, G. M., 1968, The calculation of mechanical impedances relating to an indenter vibrating on the surface of semi-infinite elastic body, *Journal of Sound and Vibration*, **8**, 215–228.
- Hatton, L., M. H. Worthington, and J. Makin, 1986, *Seismic data processing*: Blackwell Scientific Publications.
- Hudson, D. J., 1964, *Statistics*: European Center for Nuclear Studies.
- Jeffryes, B. P., 1996, Far-field harmonic measurement for seismic vibrators: 66th Annual International Meeting, SEG, Expanded Abstracts, 60–63.
- Johnson, K. L., 1985, *Contact mechanics*: Cambridge University Press.
- Korn, G. A., and T. M. Korn, 1968, *Mathematical handbook for scientists and engineers*, 2nd ed.: McGraw-Hill Book Company.
- Landau, L. D., E. M. Lifshitz, A. M. Kosevich, and L. P. Pitaevskii, 1986, *Theory of elasticity*: Pergamon Press.
- Lebedev, A. V., and I. A. Beresnev, 2004, Nonlinear distortion of signals radiated by vibroseis sources: *Geophysics*, **69**, 968–977.
- , 2005, Radiation from flexural vibrations of the baseplate and their effect on the accuracy of travel-time measurements: *Geophysical Prospecting*, **53**, 543–555.
- Lebedev, A. V., and A. I. Malekhanov, 2003, Coherent seismoacoustics: *Radiophysics and Quantum Electronics*, **46**, 523–538.
- Lerwill, W. E., 1981, The amplitude and phase response of a seismic vibrator: *Geophysical Prospecting*, **29**, 503–528.
- Liu, P., S. Hartzell, and W. Stephenson, 1995, Non-linear multiparameter inversion using a hybrid global search algorithm: Applications in reflection seismology: *Geophysical Journal International*, **122**, 991–1000.
- Merritt, H. E., 1967, *Hydraulic control systems*: John Wiley & Sons.
- Miller, G. F. and H. Pursey, 1954, The field and radiation impedance of mechanical radiators on the free surface of a semi-infinite isotropic solid: *Proceedings of the Royal Society (London)*, **A223**, 521–541.
- Rudenko, O. V., and C. A. Vu, 1994, Nonlinear acoustic properties of a rough surface contact and acoustodiagnostics of a roughness height distribution: *Acoustical Physics*, **40**, 593–596.
- Safar, M. H., 1984, On the determination of the downgoing P-waves radiated by the vertical seismic vibrator: *Geophysical Prospecting*, **32**, 392–405.
- Sallas, J. J., 1984, Seismic vibrator control and the downgoing P-wave: *Geophysics*, **49**, 732–740.
- Sallas, J. J., and R. M. Weber, 1982, Comments on “The amplitude and phase response of a seismic vibrator” by W. E. Lerwill: *Geophysical Prospecting*, **30**, 935–938.
- Sheriff, R. E., and L. P. Geldart, 1995, *Exploration seismology*: 2nd ed.: Cambridge University Press.
- Solodov, I. Y., 1998, Ultrasonic of non-linear contacts: Propagation, reflection and NDE-applications: *Ultrasonics*, **36**, 383–390.
- van der Veen, M., J. Brouwer, and K. Helbig, 1999, Weighted sum method for calculating ground force: An evaluation by using a portable vibrator system: *Geophysical Prospecting*, **47**, 251–267.